Chemical Science

RSC Publishing

EDGE ARTICLE

View Article Online
View Journal | View Issue

Cite this: *Chem. Sci.*, 2013, **4**, 2423

Engineering of thiocyanate-free Ru(II) sensitizers for high efficiency dye-sensitized solar cells†

Sheng-Wei Wang,‡[a] Kuan-Lin Wu,‡[ab] Elham Ghadiri,[b] Maria Grazia Lobello,[c] Shu-Te Ho,[a] Yun Chi,*[a] Jacques-E. Moser,*[b] Filippo De Angelis,*[c] Michael Grätzel[b] and Mohammad K. Nazeeruddin*[b]

Received 26th February 2013
Accepted 10th April 2013

DOI: 10.1039/c3sc50399b

www.rsc.org/chemicalscience

We synthesized a series of Ru(II) metal complexes **TFRS-1**, **-2**, **-4**, **-21**, **-22** and **-24** with a single 4,4′-dicarboxylic acid-2,2′-bipyridine together with two functionalized pyridyl azolate ancillary ligands consisting of pyrazolate or triazolate groups. Both photophysical measurements and DFT/TDDFT calculations were conducted to gain insight into their electronic and optical properties. The triazolate series of sensitizers **TFRS-21**, **-22** and **-24** showed an enlarged optical band gap with respect to their pyrazolate counterparts **TFRS-1**, **-2** and **-4**. When employed in dye sensitized solar cells (DSCs), the triazolate sensitizers show slightly inferior J_{SC} values due to the poor incident photon-to-current conversion efficiencies recorded compared to the pyrazolate series. Moreover, the endowed 5-(hexylthio)thiophen-2-yl substituents exert a notable hyperchromic effect and bathochromic shift in the absorption spectra, which then improves the short circuit current J_{SC} to 18.7 and 15.5 mA cm^{-2} and the overall conversion efficiency to $\eta = 10.2\%$ and 8.25% for **TFRS-4** and **TFRS-24**, respectively. For the evaluation of V_{OC}, transient photocurrent and photovoltage decay measurements were carried out to compare the rates of interfacial recombination of electrons from the TiO_2 conduction band to electrolyte.

Introduction

As the situation of global warming continues, it is becoming obvious that mankind must switch to renewable energies, which encourages our societies to place strong emphasis on the development of emerging photovoltaic technologies. However, the main barrier that prevents them from becoming the major electricity supplier is their high manufacturing costs. Fortunately, the third-generation technology, *i.e.* dye sensitized solar cells (DSCs), may provide the needed breakthrough, by virtue of their low fabrication costs and good power conversion efficiencies.[1–4] Generally speaking, a DSC consists of a tailor-made light-absorbing sensitizer deposited on a nanocrystalline TiO_2 photoanode, the I^-/I_3^- redox couple for the transport of electrical charge, and a thin layer of platinum in the counter electrode.[5–9] For the sensitizers, it has been reported that Ru(II) metal complexes exhibit superior, double-digit efficiencies under AM 1.5 global illumination.[10–15] However, the thiocyanate ligands incorporated in typical Ru(II) sensitizers are believed to provide the weakest bonding of the whole molecule, making the sensitizers and, hence, the as-fabricated solar cells somewhat unstable under excessive thermal stress and/or light soaking.[16] This latent inferiority has triggered studies attempting to replace the thiocyanate ligands of Ru(II) sensitizers with different chelating anions, such as diketonate,[17] picolinate[18] and heteroaromatic cyclometalates,[19,20] among which the cyclometalates seem to be the most promising ancillary ligands. A prominent conversion efficiency of 10.1% was documented for a tris-bidentate Ru(II) complex **YE05**, featuring a single 2,4-difluorophenyl pyridine cyclometalated ligand,[21,22] see Scheme 1.

Encouraged by this finding, many attempts have been executed to optimize the relevant cyclometalated Ru(II) complexes through modification of their structural and electrochemical properties. On the one hand, van Koten and coworkers[19,20] and Berlinguette and coworkers[23–25] utilized either tridentate or bidentate cyclometalated ligands to assemble Ru(II) sensitizers devoid of thiocyanate ligands, achieving the highest efficiency of ~8.8%.[26] On the other hand, our recent endeavors have shown that both functionalized pyridyl pyrazolate[27,28] and 2,6-dipyrazolyl pyridine[29] can be used as replacements for the aforementioned bidentate and tridentate aromatic cyclometalates. The resulting Ru(II) based sensitizers, named **TFRS-2** and **TF-2**, have shown outstanding

[a]*Department of Chemistry and Low Carbon Energy Research Center, National Tsing Hua University, Hsinchu 30013, Taiwan. E-mail: ychi@mx.nthu.edu.tw*

[b]*Laboratory of Photonics and Interfaces, Institute of Chemical Sciences and Engineering, Ecole Polytechnique Fédérale de Lausanne (EPFL), CH-1015 Lausanne, Switzerland. E-mail: mdkhaja.nazeeruddin@epfl.ch*

[c]*Computational Laboratory for Hybrid/Organic Photovoltaics (CLHYO), ISTM-CNR, Via Elce di Sotto 8, 06123, Perugia, Italy. E-mail: filippo@thch.unipg.it*

† Electronic supplementary information (ESI) available: Synthetic procedures, Fig. S1–4 and Tables S1–8. See DOI: 10.1039/c3sc50399b

‡ S-WW and K-LW contributed equally to this work.

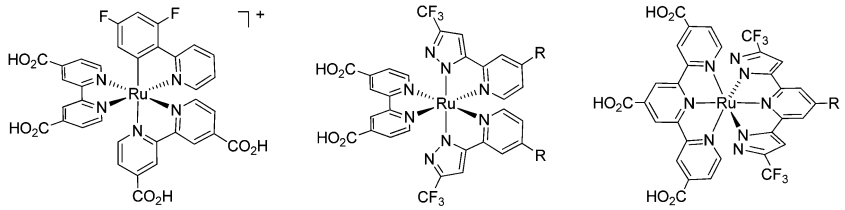

Scheme 1 Chemical structures of various thiocyanate-free Ru(II) complexes.

device performances, together with excellent device stabilities under accelerated light-soaking tests at 60 °C for over 1000 h. Herein, we report a follow-up study on the search for the best design of the **TFRS**-sensitizers that possess a series of distinctive pyridyl azolate chelates.

Results and discussion

Preparation and characterization

All **TFRS** sensitizers were synthesized using a single 4,4′-dicarboxylic acid-2,2′-bipyridine anchor plus two functionalized pyridyl azolate ancillaries. Two classes of azole fragments, *e.g.* pyrazole and 1,2,4-triazole, along with three different appendages attached at the 4-position of the pyridyl group, *i.e.* R = H, 5-hexylthiophen-2-yl and 5-(hexylthio)thiophen-2-yl, were employed for probing their combined influence on the UV-Vis spectral, electrochemical and photovoltaic properties. These variations then produced a total of six azolate chelates, for which the representative synthetic procedures are compiled in the ESI.†

The corresponding ester derivatives of the **TFRS** sensitizers were prepared by reacting Ru(diethyl 2,2′-bipyridine-4,4′-dicarboxylate)(*p*-cymene)Cl and the respective 2-pyridyl azoles in refluxing 2-methoxyethanol. In general, silica gel column chromatography was executed to separate the isomeric products, which are expected based on the statistical, random distribution of the asymmetric azoles. However, among three expected isomers, the one with *trans*-azolate fragments turned out to be the major product. The yields (28–33%) of the *trans*-pyrazolate complexes, *i.e.* **TFRS-1**, **-2** and **-4**, are notably higher than those recorded for the corresponding triazolate counterparts **TFRS-21**, **-22** and **-24** (15–20%), showing the first influence of the ancillary chelates.

Subsequently, these ester derivatives were hydrolyzed in 1 M NaOH solution at 100 °C for 24 h. The **TFRS** sensitizers were obtained by acidification and trituration with deionized water and diethyl ether in sequence. The molecular structures of these complexes are depicted in Scheme 2. It is notable that the azolate and pyridyl fragments in **TFRS-1–24** are all located at the mutual *trans*- and *cis*-dispositions, respectively reminiscent of the ligand arrangement of analogous Ru(II) and Ir(III) complexes carrying two pyridyl azolate chelates.[30,31]

The absorption spectra of pyrazolate sensitizers **TFRS-1**, **-2** and **-4** with a concentration of 1.2×10^{-5} M in DMF are depicted in Fig. 1a, for which the numerical data are summarized in Table 1. In addition to the higher energy ππ* absorptions, the parent complex **TFRS-1** exhibits two peak maxima at 405 and 515 nm, which are attributable to the metal-to-ligand charge transfer bands (MLCT) mixed with a small amount of ligand-to-ligand charge transfer contribution (*vide infra*). Moreover, upon introduction of 5-hexylthiophen-2-yl substituents to **TFRS-1**, the lower energy MLCT absorption mainly displays an increase in absorptivity and a split into two peak maxima at 481 and 516 nm upon forming **TFRS-2** and, next upon switching to the 5-(hexylthio)thiophen-2-yl group, afforded a highly intense MLCT absorption at 501 nm in forming the sensitizer **TFRS-4**. Similar variations of spectral patterns and peak maxima were observed for the triazolate series of sensitizers **TFRS-21**, **-22** and **-24**, for which their UV-Vis spectra are illustrated in Fig. 1b. As can be seen, all the triazolate analogues showed relatively blue-shifted absorptions compared to their pyrazolate counterparts. The 5-(hexylthio)thiophen-2-yl substituted **TFRS-24** sensitizer showed the most red-shifted, intense absorption with a maximum at 485 nm, for which a similar effect has been observed for the Ru(II) sensitizer **C106**.[32]

UV-Vis spectral analysis was also performed under different concentrations to reveal possible aggregation in solution as well as the proton dissociation from carboxylic acid groups. As shown in Fig. 2, the spectral profile of both **TFRS-4** and **-24** in DMF changed substantially on varying the concentration from 12 to 1.2×10^{-5} M. For **TFRS-4**, its spectral pattern at 1.2×10^{-4} M is akin to that of **TFRS-1** at a much lower concentration of 1.2×10^{-5} M, showing two well separated MLCT transitions at 430 and 550 nm, respectively. Moreover, their intensity is found to gradually decrease, together with the emergence of a new absorption band at ~500 nm upon dilution. Since the absorptions at both 430 and 550 nm involve a predominant MLCT contribution to the 4,4′-dicarboxylic acid-2,2′-bipyridine, the

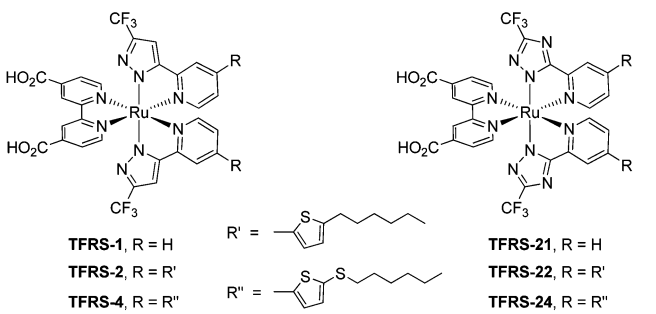

Scheme 2 Structural drawings of the studied Ru(II) sensitizers.

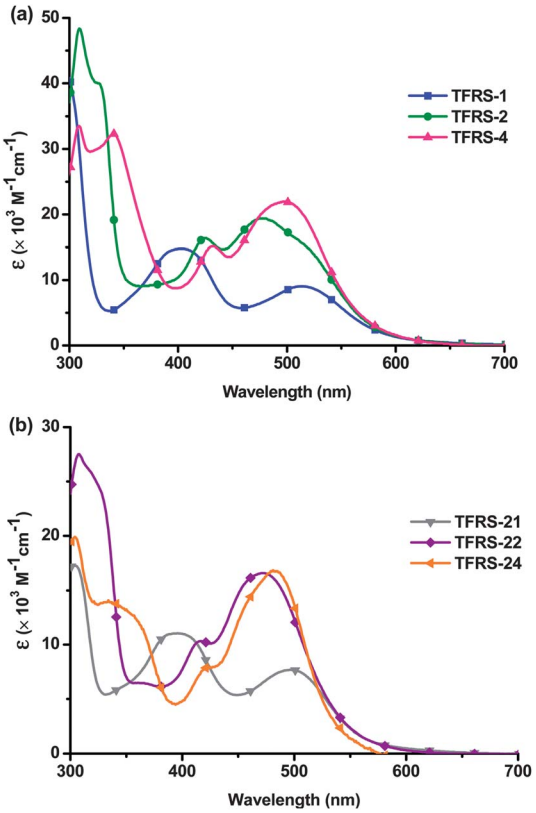

Fig. 1 (a) UV-Vis absorption spectra of 1.2×10^{-5} M solutions of **TFRS-1**, **-2** and **-4** in DMF; (b) spectra of **TFRS-21**, **-22** and **-24** recorded under identical conditions.

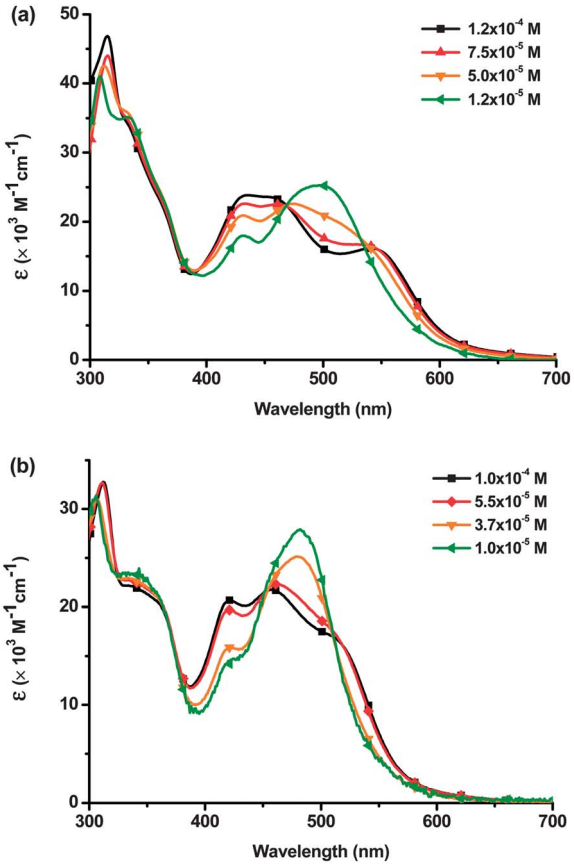

Fig. 2 UV-Vis spectra of (a) **TFRS-4** and (b) **TFRS-24** recorded in DMF at different concentrations.

decrease in intensity can be explained by the gradual dissociation of the carboxylic acid protons and the formation of carboxylates at the bipyridine anchor. The resulting negative charge on carboxylates then destabilizes the π* orbital energy of the bipyridine, which is consistent with the gradual increase in absorption intensity of the higher energy new MLCT peak at around 500 nm. In sharp contrast, minor variation of extinction coefficients is observed for the transitions above 400 nm, which are mainly due to ππ* transition, as confirmed by their greater optical densities, and independence of the solution concentration. As for the triazolate **TFRS-24**, shifting of the lowest energy MLCT band follows the same established trend, except that the variation of the extinction coefficient for all absorption bands looked more irregular compared to that of the pyrazolate analogue **TFRS-4**. We attribute this to the third nitrogen atom of the triazolate entities, which could foster bonding interactions to either the dissociated or undissociated protons from carboxylic acids.

Cyclic voltammetry was then performed to ensure that the excited state oxidation potentials ($E^{\circ\prime}$*) of the investigated complexes were sufficient for efficient injection of electrons into the conduction band of TiO_2 and to verify whether their oxidation potentials at the ground state ($E^{\circ\prime}{}_{ox}$) match the redox potential of electrolyte. As shown in Table 1, $E^{\circ\prime}{}_{ox}$, which is the potential for the Ru(II) metal oxidation, appeared in the range

Table 1 Photophysical and electrochemical data of the studied **TFRS** sensitizers

Dye	λ_{abs} [nm] ($\varepsilon \times 10^3$ [L mol^{-1} cm^{-1}])	$E^{\circ\prime}{}_{ox}{}^{a}$	E_{0-0}	$E^{\circ\prime}$*
TFRS-1	300 (40), 405 (15), 515 (9)	0.91	1.98	−1.07
TFRS-2	309 (48), 328 (40, sh), 426 (16), 481 (19, sh), 516 (15, sh)	0.90	1.91	−1.01
TFRS-4	309 (33), 341 (32), 433 (15), 501 (22)	0.93	1.97	−1.04
TFRS-21	303 (17), 396 (11), 499 (8)	1.16	2.07	−0.91
TFRS-22	308 (27), 318 (26, sh), 417 (10), 473 (17)	1.10	2.05	−0.95
TFRS-24	304 (20), 334 (14), 360 (12, sh), 429 (8), 485 (17)	1.08	2.07	−0.99

[a] Oxidation potential was measured in DMF with 0.1 M [TBA][PF_6] and with a scan rate of 50 mV s^{-1}. It was calibrated with Fc/Fc$^+$ as internal reference and converted to NHE by addition of 0.63 V.

0.90–0.93 V and 1.10–1.16 V (*vs.* NHE) for the pyrazolate derivatives **TFRS-1**, **2** and **4** and triazolate derivatives **TFRS-21**, **22** and **24**, respectively. The positive shift for **TFRS-21**, **22** and **24** is apparently caused by the more electronegative triazolate chelates. Disregarding their intrinsic difference, all data are found to be more positive than that of the I^-/I_3^- redox couple (*ca.* 0.4 V *vs.* NHE) and the hypothetical $I^-/I_2^{\cdot-}$ couple (*ca.* 0.79–0.93 V *vs.* NHE), warranting fast dye regeneration.[33–36] Next, the E_{0-0} values were determined from the intersections of the absorption and tangent of the emission peak in DMF, for which the energy gaps obtained for the triazolate sensitizers (2.05–2.07 eV) were found to be sizably larger than those of the pyrazolate counterparts (1.91–1.98 eV). The larger E_{0-0} gaps of the triazolate derivatives counterbalanced the more positive $E^{\circ\prime}_{ox}$ values, which then afforded lower $E^{\circ\prime}$* values (*i.e.* $E^{\circ\prime}_{ox} - E_{0-0}$) for triazolate derivatives **TFRS-21**, **22** and **24** (−0.91 to −0.99 V) *versus* those of the pyrazolate derivatives **TFRS-1**, **2** and **4** (−1.01 to −1.07 V), for which the trend is consistent with the electronic properties of azolates. Despite this difference, all data are more negative than the conduction band edge of the TiO_2 electrode (*ca.* −0.5 V *vs.* NHE), confirming the occurrence of fast electron injection in all cases.

Computational investigation

To gain insight into the electronic and optical properties of the investigated series of sensitizers, we performed DFT/TDDFT calculations in DMF solution on both the pyrazolate series **TFRS-1**, **-2** and **-4** and the triazolate series **TFRS-21**, **-22** and **-24**, considering for all systems a number of protons carried by the carboxylic acid anchoring groups of the 4,4′-bipyridine ranging from 0 to 2. Geometry optimizations were performed employing a 3-21G* basis set,[37] while a larger DGDZVP basis[38] was employed for the subsequent TDDFT calculations. In all cases, the B3LYP exchange-correlation functional[39] and the C-PCM solvation model[40–42] were used, as implemented in the Gaussian 09 program suite.[43]

The isodensity plots of selected molecular orbitals for the doubly protonated species of **TFRS-4** and **-24** are reported in Fig. 3, while a survey of the frontier molecular orbital energies for the investigated systems is schematically reported in Fig. 4; see also Fig. S1 and S2 as well as Tables S1 and S2 of the ESI† for the frontier orbitals and relevant data of other **TFRS** sensitizers. The HOMO is in all cases a Ru(II) t_{2g} orbital, which acquires some mixing with ligand π orbitals for the thiophene appendages. A similar mixing was found from Ru(II) sensitizers carrying π-excessive heteroaromatic substituents.[44] The localization of the LUMOs depends on the degree of protonation of the carboxy-substituted bipyridine ligand, which are the LUMOs for the protonated dyes but shifted to higher energy upon deprotonation, see below.

Within a given pyrazolate and triazolate series we notice that the LUMO energy is essentially unaltered, while the HOMO energy becomes more positive (*vs.* NHE) on going from pyrazolate **TFRS-4** and to **TFRS-24**, see Fig. 4. Upon deprotonation of the carboxylic acid groups, both the HOMOs and LUMOs are

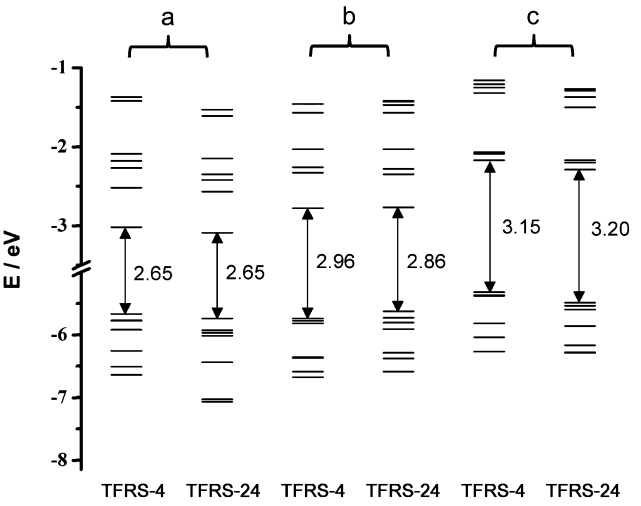

Fig. 4 Schematic representation of the energy levels of the doubly protonated (a), mono protonated (b), and doubly deprotonated (c), of **TFRS-4** and **-24** sensitizers.

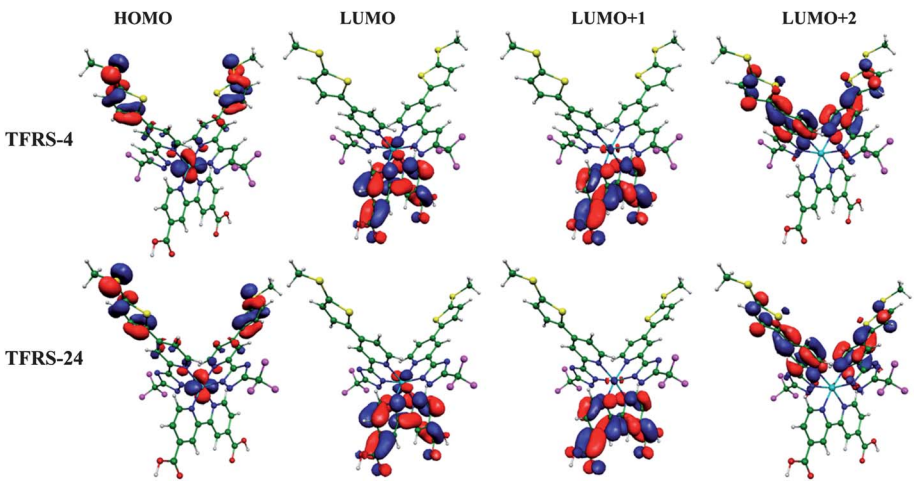

Fig. 3 Isodensity plots (isodensity value 0.035) of the HOMO and selected LUMOs of **TFRS-4** and **-24**.

shifted to less negative energies at the same time, as a result of the increased electron donation. However, the LUMOs are relatively more sensitive, so that the overall result reveals an increase of the HOMO–LUMO gap upon deprotonation.[45] Comparing homologous data for the two series of dyes, we notice that in triazolate sensitizers represented by **TFRS-24** the HOMOs are found to be *ca.* 0.2 eV lower in energy than in the corresponding pyrazolate sensitizers, in agreement with the trend of cyclic voltammetry data showing a 0.15–0.23 V shift. It is also interesting to note that the LUMOs for the triazolate sensitizers are calculated at lower energies (*ca.* 0.08 eV) compared to those of the pyrazolate series. Although not directly comparable to the $E^{\circ}*$ data reported in Table 1, our results are fully consistent with such results, showing a higher (*i.e.* more negative *vs.* the reference electrode) excited state energy for the pyrazolate series.

We now move to the optical properties of the investigated systems. The absorption spectra for the doubly protonated, mono and doubly deprotonated dyes have been computed for all the investigated species throughout the visible and UV region, thus allowing us to compare calculated and experimental data. The results for the pyrazolate and triazolate series, represented by **TFRS-4** and **TFRS-24**, are reported in Fig. 5.

As can be seen from Fig. 5, a generally good agreement is observed between calculated and experimental spectra. As could be anticipated from the HOMO–LUMO gap variation, deprotonation of the bipyridine carboxylic acid groups leads to a blue shift of the visible transitions. Interestingly, the calculated absorption spectra for the deprotonated sensitizers show a better agreement with the experimental spectra than those for the protonated analogues, suggesting that the sensitizers are effectively (partially) deprotonated in the experimental conditions. This is somehow expected, considering the substantial acidic strength of the involved carboxylic groups. It is however possible that an equilibrium among various possible deprotonated species also exists in solution, so that the resulting absorption spectrum is an average of the three differently protonated forms. A detailed analysis of the involved transitions is reported in Tables S3–S8 of the ESI;† here it suffices to note that the lowest transitions have mainly MLCT character, originating from the metal-based HOMO to the bipyridine π* LUMOs. Our calculations nicely reproduce the increased intensity experimentally observed on going from parent **TFRS-1** and **-21** to 5-hexylthiophen-2-yl substituted **TFRS-2** and **-22** and, finally, 5-(hexylthio) thiophen-2-yl substituted **TFRS-4** and **-24** sensitizers (ESI†), which is due to the admixture of metal and ligand states in the HOMOs, as discussed above. This mixture imparts a partial ligand-centered ππ* character to these otherwise pure MLCT excitations, contributing to the increased absorption intensity.

We also investigated the redox properties of the entire series of sensitizers by calculating the ground and excited state oxidation potentials of the dyes, obtained as previously described,[46] as a function of the protonation of the carboxylic groups. The results are reported in Table 2, along with experimental data converted to the vacuum scale. A general trend which can be outlined is that by decreasing the number of protons the ground state oxidation potential becomes less positive, while the lowest excitation energy (of singlet character) increases, so that a higher lying excited state oxidation potential is consistently retrieved by decreasing the number of protons carried by the carboxylic groups. We also notice that our estimated ground and excited state potentials follow the trend of the experimental data. As an example, for **TFRS-4** and **TFRS-24** our data predict a more positive ground and excited state oxidation potential at all levels of protonation for the former dye, as is found experimentally.

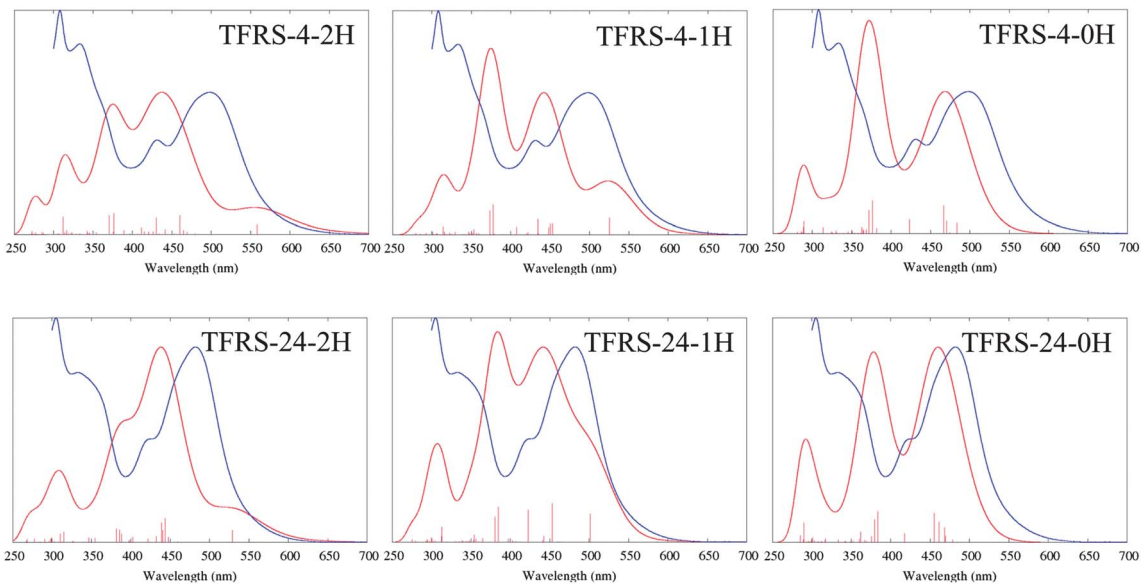

Fig. 5 Comparison between the experimental (blue lines) and calculated (red lines) (doubly protonated, left, mono protonated, center, doubly deprotonated right) optical absorption spectra for the sensitizers **TFRS-4** and **-24**. The intensities of the experimental spectra were rescaled to match those of the computed visible maximum. Vertical lines correspond to unbroadened oscillator strengths.

Table 2 Comparison of the calculated ground ($E^{\circ\prime}_{ox}$) and excited ($E^{\circ\prime}$*) state oxidation potentials of the studied **TFRS** sensitizers

		Calculated			Experimental	
Dye	#H$^+$	$E^{\circ\prime}_{ox}$ [a]	$S_0 \rightarrow S_1$	$E^{\circ\prime}$*[b]	$E^{\circ\prime}_{ox}$ [c] (V *vs.* NHE/eV *vs.* vacuum)	$E^{\circ\prime}$*[c] (V *vs.* NHE/eV *vs.* vacuum)
TFRS-1	2	5.78	1.88	3.90	0.91/5.35	−1.07/3.37
	1	5.55	1.99	3.56		
	0	5.34	2.35	2.99		
TFRS-2	2	5.75	1.87	3.88	0.90/5.34	−1.01/3.43
	1	5.53	1.98	3.55		
	0	5.32	2.34	3.01		
TFRS-4	2	5.67	1.87	3.80	0.93/5.37	−1.04/3.40
	1	5.52	1.97	3.55		
	0	5.32	2.34	2.98		
TFRS-21	2	6.01	2.03	3.98	1.16/5.60	−0.91/3.53
	1	5.77	2.14	3.63		
	0	5.57	2.51	3.06		
TFRS-22	2	5.95	2.01	3.94	1.10/5.54	−0.95/3.49
	1	5.74	2.12	3.62		
	0	5.54	2.49	3.05		
TFRS-24	2	5.74	2.00	3.74	1.08/5.52	−0.99/3.45
	1	5.63	2.12	3.51		
	0	5.49	2.48	3.01		

[a] The calculated $E^{\circ\prime}_{ox}$ values are obtained by taking the negative of the HOMO energy. [b] $E^{\circ\prime}$* is calculated as $E^{\circ\prime}_{ox} - (S_0 \rightarrow S_1)$. [c] Oxidation potentials *vs.* NHE have been converted on the vacuum scale by addition of 4.44 V.

Fabrication of devices

The DSC devices were fabricated using a 12 + 6 μm TiO_2 anode and with a 4 × 4 mm^2 working area. The photoanode was stained in the 0.3 mM dye solution in ethanol with the addition of 20% of DMSO to increase solubility. The electrolyte consists of 0.6 M PMII, 0.03 M I_2, 0.5 M *tert*-butylpyridine (TBP), 0.1 M guanidinium thiocyanate (GNCS) and 0.05 M LiI in a mixture of valeronitrile–acetonitrile with a volume ratio of 15 : 85. Device performances were measured under a 6 × 6 mm^2 shadow mask for suppressing diffused solar irradiation. As the reference, the DSC fabricated using **TFRS-1** afforded performance parameters of J_{SC} = 16.0 mA cm^{-2}, V_{OC} = 0.76 V, FF = 0.712 and η = 8.66% under AM 1.5 G simulated one-sun conditions; pertinent data are listed in Table 3. Furthermore, upon switching the sensitizer to **TFRS-2** and then to **TFRS-4**, a better set of parameters J_{SC} = 17.3 mA cm^{-2}, V_{OC} = 0.77 V and FF = 0.723, and J_{SC} = 18.7 mA cm^{-2}, V_{OC} = 0.75 mV and FF = 0.729 were achieved, affording an overall conversion efficiency of η = 9.63% and 10.2%, respectively. It seems that the reported trend is mainly derived from the increase of short-circuit current J_{SC}, which is consistent with the higher absorptivity and bathochromic shift of absorptions, by switching to the R substituents with extended π-conjugation and higher polarizability.

Table 3 The performances of DSCs measured under AM 1.5 G one sun irradiation

Dye	J_{sc} [mA cm^{-2}]	V_{oc} [V]	FF	η [%]
TFRS-1	16.0	0.76	0.712	8.66
TFRS-2	17.3	0.77	0.723	9.63
TFRS-4	18.7	0.75	0.729	10.2
TFRS-21	14.1	0.79	0.695	7.74
TFRS-22	15.4	0.74	0.728	8.30
TFRS-24	15.5	0.72	0.739	8.25
N719	17.4	0.72	0.761	9.52

The DSCs using the triazolate sensitizers **TFRS-21**, **-22** and **-24** yielded lower short-circuit current J_{SC} values to the level of 14.1–15.5 mA cm^{-2}, compared to the **TFRS-1**, **-2** and **-4** sensitizers, albeit with minor variations in the V_{OC} and FF, resulting in efficiencies in the range of 7.74 to 8.30%. The reduced J_{SC} can be rationalized by the blue-shifted absorption, which decreases the overlap with the solar spectrum and lowers the light harvesting capability.

Graphs of incident photon-to-current conversion efficiencies (IPCEs) are shown in Fig. 6a. The onsets of the IPCE spectra of pyrazolate series **TFRS-1**, **-2** and **-4** are all close to ~810 nm, and excellent IPCE performance was observed in the range from 420 to 570 nm, among which the best sensitizer is **TFRS-4**, which shows a maximum of 40% at 700 nm and steadily increases to ~72% at 600 nm and then maintains a similar IPCE efficiency until reaching 420 nm when it starts to drop. For the triazolate series **TFRS-21**, **-22** and **-24**, the onsets started only at 750 nm, but quickly went up to 40% at 640–650 nm and reached their maxima of ~70% at 550–570 nm. These trends in the IPCE clearly reveal that the triazolate sensitizers would exhibit relatively inferior J_{SC} values compared to those of the pyrazolate counterparts, and are consistent with the optical and electrochemical properties investigated in the previous section. Fig. 6b shows the photocurrent density–voltage curves of the DSC devices. The **TFRS-4** solar cells showed the best set of short-circuit current density (J_{SC}), open-circuit voltage (V_{OC}), fill factor (FF) and overall conversion efficiency (η) values which

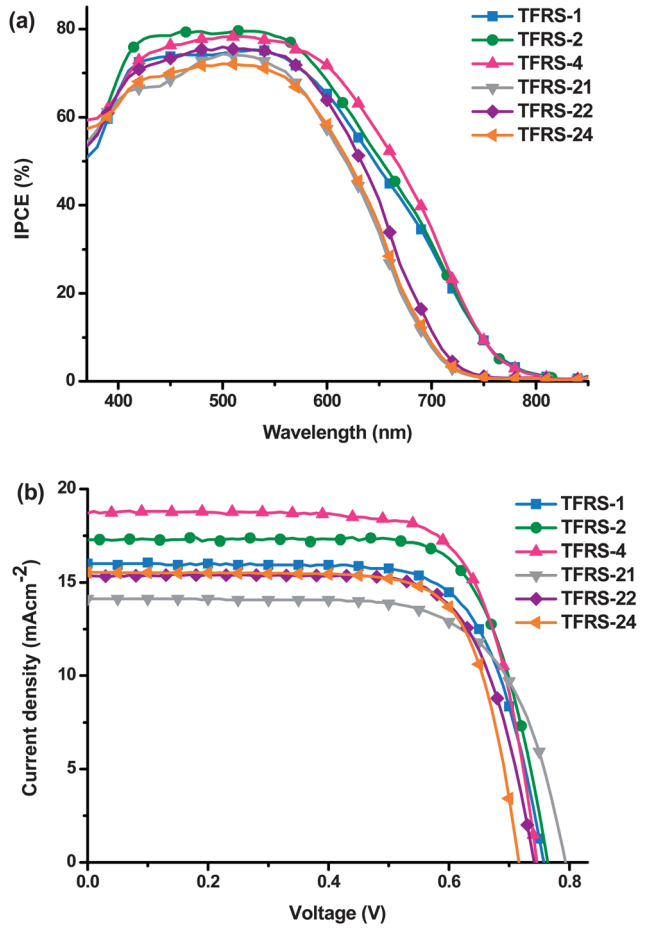

Fig. 6 (a) IPCE spectra for DSCs sensitized with various **TFRS** dyes, and (b) *J–V* characteristics measured under AM 1.5 conditions.

were measured to be 18.7 mA cm^{-2}, 0.75 V, 0.729 and 10.2%, respectively. These results are notably better than those of control devices of its kind. For instance, the cells with **TFRS-1** and **-2** sensitizers afford $J_{SC} = 16.0$ and 17.3 mA cm^{-2}, $V_{OC} =$ 0.76 and 0.77 V, and FF = 0.712 and 0.723, corresponding to an overall $\eta = 8.66$ and 9.63%. These data are comparable to our original data,[28] although they were initially recorded without the shading mask, such that the quoted performances of **TFRS-1** and **-2** are approximately 6% lower than that of **TFRS-4**, which stands as the best sensitizer for this class of materials.

However, we wish to point out that the pyrazolate series of sensitizers **TFRS-1** to **-4** all showed much superior device performances *versus* those of their triazolate counterparts **TFRS-21** to **-24**. This trend is in sharp contrast to that of the recently reported analogues **TFRS-11** to **-14**, for which the conjugated 4,4′-dicarboxyvinyl-2,2′-bipyridine is employed as the anchoring group.[47] It is believed that the extra pairs of vinyl groups on **TFRS-11** to **-14** destabilize their ground state oxidation potentials, which are verified by respective electrochemical studies. Thus, **TFRS-11** to **-14** sensitizers will need more electron deficient triazolate fragments to bring down the ground state oxidation potential and to allow a sufficient driving force for efficient dye regeneration.

Transient photocurrent and photovoltage decay measurements were carried out in order to investigate the rates of interfacial recombination of electrons from the TiO_2 conduction band to the electrolyte. It is worth noting that V_{OC} decays are measurements dependent on the accumulated charge at the TiO_2 conduction band, and hence, to obtain a fair comparison of the e^-–TiO_2/electrolyte$^+$ recombination dynamics between different dyes, the charge density on both dyes must be equal. The densities of states (DOS) of the films loaded with the **TFRS-4** and **TFRS-24** sensitizers were determined from transient photocurrent decay measurements. As presented in Fig. 7a, the chemical capacitance Cμ of devices rises exponentially with the increased V_{OC}. Cμ is directly proportional to the density of state (DOS) (Cμ = q(e)DOS, where q(e) is electron charge).[48,49] It is clear that very similar electron densities are measured for the two between **TFRS-4** and **-24** sensitizers, which served as representative examples for all **TFRS** sensitizers. This observation means we can discard the contribution of a conduction band shift to the observed decrease in the back-electron transfer rate. The electron lifetimes were measured at identical electron densities using transient photovoltage measurements. Fig. 7b illustrates electron lifetime as a function of V_{OC} for the different

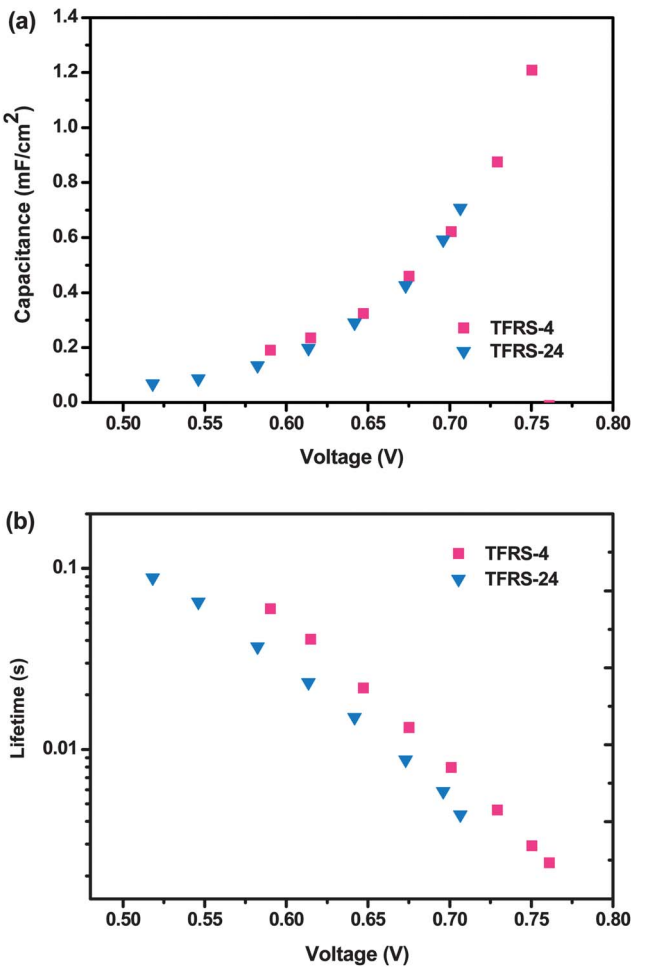

Fig. 7 Electron (a) capacitance and (b) lifetime determined with photocurrent and photovoltage decay measurements of devices with **TFRS-4** and **-24**.

sensitizers. The V_{OC} was adjusted by varying the intensity of the bias light impinging on the cell. The trend correlates rather well with the V_{OC} values obtained for these devices, *i.e.* as electron lifetime gets shorter, the V_{OC} decreases. Longer electron lifetimes were observed for **TFRS-4**, compared to **TFRS-24**. The difference was explained by the iodine binding ability with the pyrazolate and triazolate chelate, leading to faster recombination.[50–52]

The electron injection process was studied using femtosecond transient absorption spectroscopy techniques on representative pyrazolate **TFRS-4** and triazolate **TFRS-24** sensitizers, see Fig. 8. The electron injection process in two identical samples of pyrazolate and triazolate series superimposes quite well and showed no obvious difference at all.

Although the LUMO level has been slightly shifted, this has not affected the overall electron injection process. These data support the DFT simulations where the extension of the LUMO is observed to be similar in both cases. To gain an insight into the dye regeneration process having these thiocyanate-free sensitizers, and the electron back reaction process, nanosecond flash photolysis measurements were performed on both series. The dynamics of the oxidized state of the dye after its initial generation were monitored by measuring transient changes of its optical absorption at the wavelength $\lambda = 720$ nm. In the absence of a redox mediator, that is, in pure 3-methoxypropionitrile (MPN) solvent and without the redox couple, the decay of the absorption signal recorded at 720 nm reflects the dynamics of the recombination of injected electrons with S^+. In Fig. 9a, the black curve decays with a typical lifetime $\tau = 1$ ms for both **TFRS-4** and **TFRS-24**. In the presence of the redox couple, the decay of the oxidized dye signal was significantly accelerated. The fits to first exponential functions give rate constants of 59 000 s^{-1} and 110 000 s^{-1}, giving half life times of 17 and 9 μs for dye regeneration on **TFRS-4** and **TFRS-24** respectively. Although the efficient regeneration rate in is in agreement with photovoltaic measurements and a higher dye regeneration on **TFRS-24** with respect to **TFRS-4** is in agreement with the more positive oxidation potential, it should be noted that in iodide based redox electrolytes, dye regeneration is a two electron transfer process and it cannot be simply directly linked to the thermodynamics of the system.

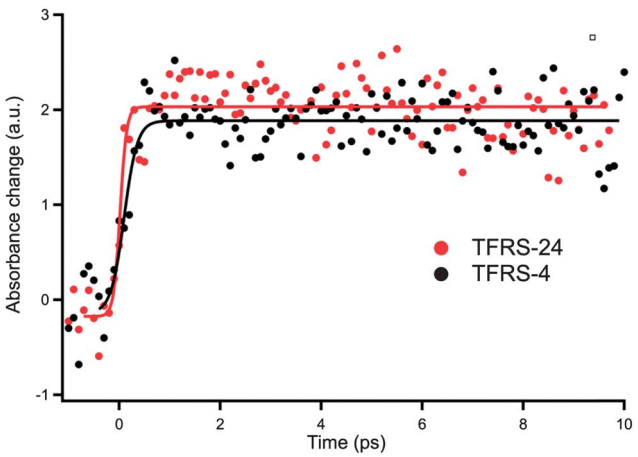

Fig. 8 Transient absorbance kinetics of **TFRS-4** and **TFRS-24**, adsorbed on a nanocrystalline TiO_2 film in the presence of redox inactive medium monitored at 720 nm, reflecting ultrafast electron injection from dye to the conduction band of TiO_2.

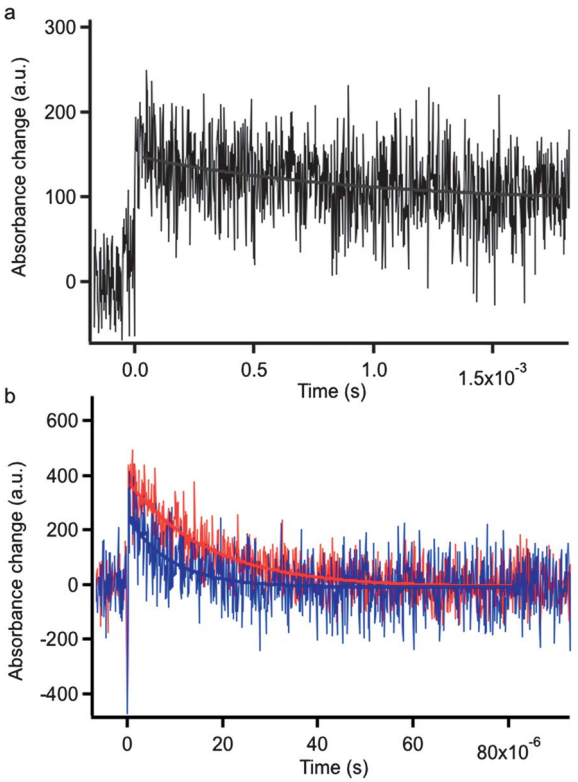

Fig. 9 Transient absorbance decay kinetics of the oxidized state of dye adsorbed on a TiO_2 nanocrystalline film (a) in the presence of MPN solvent (black) and (b) iodide based electrolyte for **TFRS-4** and **TFRS-24** highlighted in red and blue respectively. The solid lines are fits to first order exponential functions giving fitting rate constants of 60 000 s^{-1} and 110 000 s^{-1} respectively for **TFRS-4** and **TFRS-24**.

Conclusion

Ru(II) metal complexes with a 4,4′-dicarboxylic acid-2,2′-bipyridine anchor and two functionalized 2-pyridyl azolate ancillaries were systemically modified with the goal of finding better and more stable sensitizers for DSC applications. The sensitizer **TFRS-4**, featuring a hexylthiothiophene appendage on pyrazolate chelates, shows a distinctive red-shifted MLCT absorption, which improves the light-capturing ability in the visible and near infrared regions resulting in the best overall conversion efficiency ($\eta = 10.2\%$) among all sensitizers studied. In sharp contrast, the triazolate sensitizers **TFRS-21**, **-22** and **-24** exhibit relatively inferior J_{SC} and V_{OC} values compared to those of the pyrazolate counterparts due to the enlarged optical gap caused by the electron withdrawing behaviour of triazolate chelates, and the possible interaction between the triazolate group of the sensitizer and iodine in the electrolyte that induced the rapid charge recombination. Finally, despite the need for more research, **TFRS-4** could be useful for future pilot applications, based on the performance data shown in this work.

Experimental section

General synthetic procedures

All reactions were performed under an argon atmosphere and solvents were distilled from appropriate drying agents prior to use. Commercially available reagents were used without further purification unless otherwise stated. All reactions were monitored using pre-coated TLC plates (0.20 mm with fluorescent indicator UV254). Mass spectra were obtained on a JEOL SX-102A instrument operating in electron impact (EI) or fast atom bombardment (FAB) mode. ^{1}H NMR spectra were recorded on a Varian Mercury-400 or an INOVA-500 instrument. Elemental analysis was carried out with a Heraeus CHN–O rapid elementary analyzer.

Synthesis of TFRS-4

4-(5-(Hexylthio)thiophen-2-yl)-2-(3-(trifluoromethyl)-1*H*-pyrazol-5-yl)pyridine (145 mg, 0.35 mmol), Ru(diethyl 2,2′-bipyridine-4,4′-dicarboxylate)(*p*-cymene)Cl (100 mg, 0.17 mmol) and sodium acetate (98 mg, 1.00 mmol) were dissolved in 2-methoxyethanol (20 mL), and the reaction mixture was heated to reflux under stirring overnight. After evaporating the solvent, the aqueous phase was separated and extracted with dichloromethane (3 × 25 mL). The crude compound was purified by silica gel column chromatography eluting with a 3 : 2 mixture of hexane and ethyl acetate. Finally, the resulting solid was dissolved in a mixture of acetone (5 mL) and 1 M NaOH solution (5 mL). The solution was heated to reflux under N_2 for 12 h. After completing the hydrolysis, the solvent was removed and the solid was dissolved in water (10 mL) and titrated with 2 M HCl to pH 3 to afford a brown precipitate. This brown product was washed with ethyl acetate and acetone in sequence, yield: 67 mg, 33%.

Spectral data of TFRS-4

MS (FAB, ^{102}Ru): *m*/*z* 1167 $(M)^+$. ^{1}H NMR (400 MHz, d_6-DMSO, 298 K): δ 8.95 (s, 2H), 8.24 (d, J = 6.0 Hz, 4H), 7.80 (d, J = 4.0 Hz, 2H), 7.76 (dd, J = 1.6, 6.0 Hz, 2H), 7.45–7.43 (m, 4H), 7.21 (d, J = 4.0 Hz, 2H), 7.04 (d, J = 6.0 Hz, 2H), 2.89 (t, J = 7.2 Hz, 4H), 1.57–1.49 (m, 4H), 1.35–1.15 (m, 12H), 0.79 (t, J = 7.0 Hz, 6H). Anal. calcd for $C_{50}H_{46}F_6N_8O_4RuS_4 \cdot 3H_2O$: C, 49.21; N, 9.18, H, 4.30. Found: C, 48.98; N, 8.97, H, 4.01%.

Synthesis of TFRS-21

A similar procedure was used as described for **TFRS-4**, starting from 3-trifluoromethyl-5-(2-pyridyl)triazole (75 mg, 0.350 mmol). The residue was purified by silica gel column chromatography and eluting with a 3 : 2 mixture of hexane and ethyl acetate. The sensitizer **TFRS-21** was obtained as a dark red solid; yield: 25 mg, 20%.

Spectral data of TFRS-21

MS (FAB, ^{102}Ru): *m*/*z* 772 $(M)^+$. ^{1}H NMR (400 MHz, d_6-DMSO, 298 K): δ 9.01 (s, 2H), 8.10 (t, J = 8.0 Hz, 4H), 7.97 (t, J = 7.6 Hz, 2H), 7.79 (d, J = 6.0 Hz, 2H), 7.24 (t, J = 7.2 Hz, 4H), 7.33 (d, J = 6.0 Hz, 2H). Anal. calcd for $C_{28}H_{16}F_6N_{10}O_4Ru \cdot 2H_2O$: C, 41.64 N, 17.34; H, 2.50. Found: C, 41.64; N, 16.84; H, 2.62%.

Synthesis of TFRS-22 and -24

These sensitizers were obtained as a dark red solid in 18% and 15% yield, respectively.

Spectral data of TFRS-22

MS (FAB, ^{102}Ru): *m*/*z* 1104 $(M)^+$. ^{1}H NMR (400 MHz, d_6-DMSO, 298 K): δ 9.01 (s, 2H), 8.23 (d, J = 6.0 Hz, 4H), 8.17 (s, 2H), 7.81–7.79 (m, 4H), 7.63 (dd, J = 1.6, 8.0 Hz, 2H), 7.23 (d, J = 6.0 Hz, 2H), 6.94 (d, J = 3.2 Hz, 2H), 2.80 (t, J = 7.2 Hz, 4H), 1.61–1.55 (m, 4H), 1.23 (s, 12H), 0.81 (t, J = 6.0 Hz, 6H). Anal. calcd for $C_{48}H_{44}F_6N_{10}O_4RuS_2 \cdot 3H_2O$: C, 49.78; N, 12.09; H, 4.35. Found: C, 49.61; N, 11.74; H, 4.36%.

Spectral data of TFRS-24

MS (FAB, ^{102}Ru): *m*/*z* 1169 $(M)^+$. ^{1}H NMR (400 MHz, d_6-DMSO, 298 K): δ 9.04 (d, J = 1.6, 2H), 8.26 (d, J = 6.0 Hz, 2H), 8.22 (d, J = 2.4, 2H), 7.92 (d, J = 4.0, 2H), 7.82 (dd, J = 1.6, 8.0 Hz, 2H), 7.68 (dd, J = 2.0, 4.0 Hz, 2H), 7.27 (d, J = 6.0 Hz, 2H), 7.23 (d, J = 4.0 Hz, 2H), 2.94 (t, J = 7.2 Hz, 4H), 1.60–1.53 (m, 4H), 1.39–1.20 (m, 12H), 0.82 (t, J = 6.9 Hz, 6H). Anal. calcd for $C_{48}H_{44}F_6N_{10}O_4RuS_4 \cdot 2H_2O$: C, 47.87; N, 11.63; H, 4.02. Found: C, 47.70; N, 11.42; H, 4.01%.

Device fabrication

Fluorine-doped tin oxide (FTO) coated glasses (3.2 mm thickness, sheet resistance of 9 Ω cm^{-2}, Pilkington) were washed with detergent, water, acetone and ethanol, sequentially. After treatment in a UV-O_3 system for 15 min (PSD series UV-ozone cleaning, Novascan Technologies, Inc.), the FTO glass plates were immersed into a 40 mM aqueous $TiCl_4$ solution at 70 °C for 30 min and rinsed with water and ethanol. The photoanodes composed of nanocrystalline TiO_2 were prepared using literature procedures.[53] The TiO_2 electrodes of 12 μm thickness were deposited on transparent conducting glass, on which a 6 μm light-scattering layer containing 400 nm TiO_2 particles (PST-400, JGC Catalysts and Chemicals, Japan) was screen-printed (active area, 0.16 cm^2). The TiO_2 electrodes were heated under an air flow at 325 °C for 30 min, followed by heating at 375 °C for 5 min, 450 °C for 15 min, and 500 °C for 30 min. The TiO_2 electrodes were treated with a 40 mM aqueous solution of $TiCl_4$ at 70 °C for 30 min and then washed with water and ethanol. The electrodes were sintered again at 500 °C for 30 min and left to cool to 80 °C before dipping them into the dye solution (0.3 mM) for 18 h at 25 °C. The dye solution was prepared in absolute ethanol with 20% (v/v) dimethyl sulfoxide (DMSO). The Pt-coated counter electrodes were prepared using a 5 mM H_2PtCl_6 solution in isopropyl alcohol, followed by heating at 400 °C for 15 min. The dye sensitized TiO_2 electrodes were assembled with Pt counter electrodes by inserting a hot-melt Surlyn film (Meltonix 1170–25, 25 μm, Solaronix) as spacer. The electrolyte solution, which consists of 0.6 M 1-methyl-3-propylimidazolium iodide (PMII), 0.03 M iodine, 0.5 M

tert-butylpyridine (TBP), 0.1 M guanidinium thiocyanate (GNCS) and 0.05 M LiI in a 15 : 85 (v/v) mixture of valeronitirile and acetonitrile, was injected into the cell through a pre-drilled hole at the counter electrode. Finally, the hole was sealed using a hot-melt Surlyn film and a cover glass. In order to reduce scattered light from the edges of glass electrodes of the dyed TiO_2 layer,[54] all devices were covered with a light-shading mask with a size of 0.6×0.6 cm^2.

Photovoltaic characterization

Photovoltaic measurements were recorded with a Newport Oriel Class A Solar Simulator (Model 91159) equipped with a class A 150 W xenon light source powered by a Newport power supply (Model 69907). The light output (area: 2×2 in^2) was calibrated to AM 1.5 using a Newport Oriel correction filter to reduce the spectra mismatch in the region of 350–750 nm to less than 4%. The power output of the lamp was measured to 1 Sun (100 mW cm^{-2}) using a certified Si reference cell (SRC-1000 TC-QZ, VLSI standard S/N: 10510-0031). The current voltage characteristic of each cell was obtained by applying an external potential bias to the cell and measuring the generated photocurrent with a Keithley digital source meter (Model 2400). The spectra of incident photon-to-current conversion efficiency (IPCE) were calculated with the equation of $1240 J_{SC}(\lambda)/(\lambda P_{in}(\lambda))$ and were plotted as a function of incident wavelength with an increment of 10 nm. It should be noted that 20 sets of J_{SC} (interval 50 ms) were collected after each illumination of 3 s and were averaged for the calculations of IPCE.[55] A 300 W Xe lamp (Model 6258, Newport Oriel) combined with an Oriel cornerstone 260 1/4 m monochromator (Model 74100) provided an unchopped monochromatic beam onto a photovoltaic cell. The beam intensity was calibrated with a power meter (Model 1936 C, Newport) equipped with a Newport 818-UV photodetector. Photovoltaic performance was measured using a metal mask with an aperture area of 0.36 cm^2.

Laser spectroscopy

Dye-loaded, 3 μm-thick transparent nanocrystalline TiO_2 films were used to study electron injection, electron back reaction and dye regeneration processes using a nanosecond and femtosecond transient absorption spectrophotometer. Pulsed excitation (λ) 550 nm, 5 ns fwhm pulse duration, 20 μJ cm^{-2} pulse energy fluence, 30 Hz repetition rate was provided by an optical parametric oscillator (OPO, GWU OPO-355) pumped by a frequency-tripled, Q-switched Nd:YAG laser (Continuum, Powerlite 7030). These conditions ensure that, at most, one electron is injected per TiO_2 particle at a time. The probe light from a Xe arc lamp was passed through filters, various optical elements, the sample, and a second grating monochromator, before being detected by a fast photomultiplier tube and recorded by a digital oscilloscope. The transient probe signal measured at $\lambda =$ 700 nm corresponds to the time evolution of the absorbance of the oxidized state of the dye (S^+) as deduced from previously recorded transient absorption spectra. The transient decay observed corresponds to the lifetime of S^+ in the presence or absence of a redox electrolyte. Traces were obtained by averaging over 3000 laser shots.

Acknowledgements

MGL and FDA thank FP7-ENERGY-2010 project 261920 "ESCORT" for financial support, while YC thanks the National Science Council of Taiwan for funding. KLW is a recipient of the Graduate Students Study Abroad Program sponsored by the National Science Council of Taiwan (NSC-101-2917-I-007-017).

Notes and references

1 N. Robertson, *Angew. Chem., Int. Ed.*, 2008, **47**, 1012.
2 L. M. Goncalves, V. de Zea Bermudez, H. A. Ribeiro and A. M. Mendes, *Energy Environ. Sci.*, 2008, **1**, 655.
3 M. Grätzel, *Acc. Chem. Res.*, 2009, **42**, 1788.
4 A. Hagfeldt, G. Boschloo, L. Sun, L. Kloo and H. Pettersson, *Chem. Rev.*, 2010, **110**, 6595.
5 J. R. Durrant, S. A. Haque and E. Palomares, *Chem. Commun.*, 2006, 3279.
6 L. M. Peter, *J. Phys. Chem. C*, 2007, **111**, 6601.
7 Y. Luo, D. Li and Q. Meng, *Adv. Mater.*, 2009, **21**, 4647.
8 S. Ardo and G. J. Meyer, *Chem. Soc. Rev.*, 2009, **38**, 115.
9 J. Preat, D. Jacquemin and E. A. Perpete, *Energy Environ. Sci.*, 2010, **3**, 891.
10 C.-Y. Chen, M. Wang, J.-Y. Li, N. Pootrakulchote, L. Alibabaei, C.-H. Ngoc-Le, J.-D. Decoppet, J.-H. Tsai, C. Grätzel, C.-G. Wu, S. M. Zakeeruddin and M. Grätzel, *ACS Nano*, 2009, **3**, 3103.
11 Q. Yu, S. Liu, M. Zhang, N. Cai, Y. Wang and P. Wang, *J. Phys. Chem. C*, 2009, **113**, 14559.
12 F. Sauvage, D. Chen, P. Comte, F. Huang, L.-P. Heiniger, Y.-B. Cheng, R. A. Caruso and M. Grätzel, *ACS Nano*, 2010, **4**, 4420.
13 F. Sauvage, S. Chhor, A. Marchioro, J.-E. Moser and M. Grätzel, *J. Am. Chem. Soc.*, 2011, **133**, 13103.
14 S.-Q. Fan, C. Kim, B. Fang, K.-X. Liao, G.-J. Yang, C.-J. Li, J.-J. Kim and J. Ko, *J. Phys. Chem. C*, 2011, **115**, 7747.
15 J.-J. Kim, H. Choi, S. Paek, C. Kim, K. Lim, M.-J. Ju, H. S. Kang, M.-S. Kang and J. Ko, *Inorg. Chem.*, 2011, **50**, 11340.
16 P. T. Nguyen, R. Degn, H. T. Nguyen and T. Lund, *Sol. Energy Mater. Sol. Cells*, 2009, **93**, 1939.
17 A. Islam, F. A. Chowdhury, Y. Chiba, R. Komiya, N. Fuke, N. Ikeda, K. Nozaki and L. Han, *Chem. Mater.*, 2006, **18**, 5178.
18 T. Funaki, M. Yanagida, N. Onozawa-Komatsuzaki, K. Kasuga, Y. Kawanishi and H. Sugihara, *Chem. Lett.*, 2009, **38**, 62.
19 S. H. Wadman, J. M. Kroon, K. Bakker, M. Lutz, A. L. Spek, G. P. M. van Klink and G. van Koten, *Chem. Commun.*, 2007, 1907.
20 S. H. Wadman, J. M. Kroon, K. Bakker, R. W. A. Havenith, G. P. M. van Klink and G. van Koten, *Organometallics*, 2010, **29**, 1569.
21 T. Bessho, E. Yoneda, J.-H. Yum, M. Guglielmi, I. Tavernelli, H. Imai, U. Rothlisberger, M. K. Nazeeruddin and M. Grätzel, *J. Am. Chem. Soc.*, 2009, **131**, 5930.
22 F. De Angelis, S. Fantacci, A. Selloni, M. K. Nazeeruddin and M. Grätzel, *J. Phys. Chem. C*, 2010, **114**, 6054.

23 P. G. Bomben, K. C. D. Robson, P. A. Sedach and C. P. Berlinguette, *Inorg. Chem.*, 2009, **48**, 9631.
24 B. D. Koivisto, K. C. D. Robson and C. P. Berlinguette, *Inorg. Chem.*, 2009, **48**, 9644.
25 P. G. Bomben, K. D. Theriault and C. P. Berlinguette, *Eur. J. Inorg. Chem.*, 2011, 1806.
26 P. G. Bomben, T. J. Gordon, E. Schott and C. P. Berlinguette, *Angew. Chem., Int. Ed.*, 2011, **50**, 10682.
27 B.-S. Chen, K. Chen, Y.-H. Hong, W.-H. Liu, T.-H. Li, C.-H. Lai, P.-T. Chou, Y. Chi and G.-H. Lee, *Chem. Commun.*, 2009, 5844.
28 K.-L. Wu, H.-C. Hsu, K. Chen, Y. Chi, M.-W. Chung, W.-H. Liu and P.-T. Chou, *Chem. Commun.*, 2010, **46**, 5124.
29 C.-C. Chou, K.-L. Wu, Y. Chi, W.-P. Hu, S. J. Yu, G.-H. Lee, C.-L. Lin and P.-T. Chou, *Angew. Chem., Int. Ed.*, 2011, **50**, 2054.
30 Y. L. Tung, L. S. Chen, Y. Chi, P. T. Chou, Y. M. Cheng, E. Y. Li, G. H. Lee, C. F. Shu, F. I. Wu and A. J. Carty, *Adv. Funct. Mater.*, 2006, **16**, 1615–1626.
31 P.-T. Chou and Y. Chi, *Chem.–Eur. J.*, 2007, **13**, 380–395.
32 Y. Cao, Y. Bai, Q. Yu, Y. Cheng, S. Liu, D. Shi, F. Gao and P. Wang, *J. Phys. Chem. C*, 2009, **113**, 6290.
33 D. Kuciauskas, M. S. Freund, H. B. Gray, J. R. Winkler and N. S. Lewis, *J. Phys. Chem. B*, 2001, **105**, 392.
34 J. N. Clifford, E. Palomares, M. K. Nazeeruddin, M. Grätzel and J. R. Durrant, *J. Phys. Chem. C*, 2007, **111**, 6561.
35 A. Listorti, B. O'Regan and J. R. Durrant, *Chem. Mater.*, 2011, **23**, 3381.
36 G. Boschloo, E. A. Gibson and A. Hagfeldt, *J. Phys. Chem. Lett.*, 2011, **2**, 3016.
37 J. S. Binkley, J. A. Pople and W. J. Hehre, *J. Am. Chem. Soc.*, 1980, **102**, 939.
38 N. Godbout, D. R. Salahub, J. Andzelm and E. Wimmer, *Can. J. Chem.*, 1992, **70**, 560.
39 A. D. Becke, *J. Chem. Phys.*, 1993, **98**, 5648.
40 S. Miertus, E. Scrocco and J. Tomasi, *Chem. Phys.*, 1981, **55**, 117.
41 M. Cossi, V. Barone, R. Cammi and J. Tomasi, *Chem. Phys. Lett.*, 1996, **255**, 327.
42 M. Cossi and V. Barone, *J. Chem. Phys.*, 2001, **115**, 4708.
43 M. J. Frisch, G. W. Trucks, H. B. Schlegel, G. E. Scuseria, M. A. Robb, J. R. Cheeseman, G. Scalmani, V. Barone, B. Mennucci, G. A. Petersson, H. Nakatsuji, M. Caricato, X. Li, H. P. Hratchian, A. F. Izmaylov, J. Bloino, G. Zheng, J. L. Sonnenberg, M. Hada, M. Ehara, K. Toyota, R. Fukuda, J. Hasegawa, M. Ishida, T. Nakajima, Y. Honda, O. Kitao, H. Nakai, T. Vreven, J. A. Montgomery, Jr., J. E. Peralta, F. Ogliaro, M. Bearpark, J. J. Heyd, E. Brothers, K. N. Kudin, V. N. Staroverov, R. Kobayashi, J. Normand, K. Raghavachari, A. Rendell, J. C. Burant, S. S. Iyengar, J. Tomasi, M. Cossi, N. Rega, J. M. Millam, M. Klene, J. E. Knox, J. B. Cross, V. Bakken, C. Adamo, J. Jaramillo, R. Gomperts, R. E. Stratmann, O. Yazyev, A. J. Austin, R. Cammi, C. Pomelli, J. Ochterski, R. L. Martin, K. Morokuma, V. G. Zakrzewski, G. A. Voth, P. Salvador, J. J. Dannenberg, S. Dapprich, A. D. Daniels, O. Farkas, J. B. Foresman, J. V. Ortiz, J. Cioslowski and D. J. Fox, *GAUSSIAN 09 (Revision A.1)*, Gaussian, Inc., Wallingford, CT, 2009.
44 A. Abbotto, C. Barolo, L. Bellotto, F. De Angelis, M. Grätzel, N. Manfredi, C. Marinzi, S. Fantacci, J.-H. Yum and M. K. Nazeeruddin, *Chem. Commun.*, 2008, 5318.
45 F. De Angelis, S. Fantacci and A. Selloni, *Chem. Phys. Lett.*, 2004, **389**, 204.
46 A. Filippo De, F. Simona and S. Annabella, *Nanotechnology*, 2008, **19**, 424002.
47 K.-L. Wu, W.-P. Ku, S.-W. Wang, A. Yella, Y. Chi, S.-H. Liu, P.-T. Chou, M. K. Nazeeruddin and M. Graetzel, *Adv. Funct. Mater.*, 2013, DOI: 10.1002/adfm.201201876.
48 B. C. O'Regan, K. Bakker, J. Kroeze, H. Smit, P. Sommeling and J. R. Durrant, *J. Phys. Chem. B*, 2006, **110**, 17155–17160.
49 B. C. O'Regan and J. R. Durrant, *J. Phys. Chem. B*, 2006, **110**, 8544–8547.
50 B. C. O'Regan, K. Walley, M. Juozapavicius, A. Anderson, F. Matar, T. Ghaddar, S. M. Zakeeruddin, C. d. Klein and J. R. Durrant, *J. Am. Chem. Soc.*, 2009, **131**, 3541–3548.
51 H. Kusama and H. Sugihara, *J. Photochem. Photobiol., A*, 2007, **187**, 233–241.
52 H. Kusama and H. Arakawa, *J. Photochem. Photobiol., A*, 2004, **164**, 103–110.
53 S. Ito, T. N. Murakami, P. Comte, P. Liska, C. Grätzel, M. K. Nazeeruddin and M. Grätzel, *Thin Solid Films*, 2008, **516**, 4613.
54 S. Ito, K. Nazeeruddin, P. Liska, P. Comte, R. Charvet, P. Pechy, M. Jirousek, A. Kay, S. M. Zakeeruddin and M. Grätzel, *Progr. Photovolt.: Res. Appl.*, 2006, **14**, 589.
55 X.-Z. Guo, Y.-H. Luo, Y.-D. Zhang, X.-C. Huang, D.-M. Li and Q.-B. Meng, *Rev. Sci. Instrum.*, 2010, **81**, 103106.